Rheology of Concentrated Isotropic and Anisotropic Xanthan Solutions. 2. A Semiflexible Wormlike Intermediate Molecular Weight Sample

Hu-Cheng Lee and David A. Brant*

Department of Chemistry, University of California, Irvine, California 92697-2025

Received August 28, 2001

ABSTRACT: The rheology of a semiflexible wormlike xanthan sample (Fraction X2F2, $M_w = 4.80 \times 10^5$ g/mol) has been studied in oscillatory and steady shear modes in aqueous NaCl (0.01, 0.1, 1.0 M) at polymer concentrations spanning the isotropic, biphasic, and fully anisotropic regimes. The rheological observables change with polymer weight fraction W and shear rate/frequency in much the same way as described in the companion paper for lower molecular weight sample X13F3 ($M_w = 1.54 \times 10^5$ g/mol). This semiflexible, intermediate molecular weight sample is more readily aligned under the steady shear field than the rodlike, low molecular weight sample X13F3. For the anisotropic solutions, the steady shear viscosity η shows shear thinning behavior at high and low shear rate $\dot{\gamma}$ and shear thickening at intermediate $\dot{\gamma}$, unusual behavior that is presumably linked to the negative first normal stress difference sometimes seen in lyotropic liquid crystalline systems. A plot against W of the crossover frequency ω_c at which the loss tangent is unity is "V" shaped with the minimum corresponding to the phase boundary concentration between the isotropic and biphasic regions. The Cox−Merz rule is generally not obeyed. The dynamic viscosity $\eta^* > \eta$ at most frequencies for systems that are isotropic or predominantly isotropic; the situation is reversed in anisotropic or predominantly anisotropic systems. In contrast to observations for X13F3, η and η^* are sensitive to salt concentration in the isotropic as well as the anisotropic phase. Estimates of the mean separation of xanthan molecules in the equilibrium anisotropic phase show that separations exceed those at which hydration forces between biological macromolecules are postulated to be dominant. Electrostatic interactions play a prominent role in dictating the concentrations of the coexisting isotropic and anisotropic phases.

Introduction

In the preceding paper,[1] we reported a steady shear and oscillatory rheological study of rigid, rodlike aqueous xanthan fraction X13F3 ($M_w = 1.54 \times 10^5$ g/mol, $M_w/M_n = 1.1$, $L/2q \approx 0.33$). (See the preceding paper for definitions of these and other symbols employed here.) Here we present the results of a similar study for an intermediate molecular weight xanthan fraction X2F2 ($M_w = 4.80 \times 10^5$ g/mol, $M_w/M_n = 1.2$, $L/2q \approx 1.03$). We consider again polymer concentrations spanning the domain of solutions that are isotropic, anisotropic, and biphasic in the absence of shear. Fraction X2F2 falls between the rigid rodlike limit and the very high molecular weight flexible chain limit and can be considered a semiflexible, wormlike chain. We report measurements of η, η^*, G', and G'' as functions of C_s, W, $\dot{\gamma}$, and ω. Similarities, and differences, between the two samples are highlighted. A review of previous rheological studies of aqueous xanthan in the dilute, semidilute, and concentrated regimes is presented in the companion paper.

Experimental Section

All experimental details are given in the previous paper,[1] where the physical characteristics of fraction X2F2 are reported in Table 1.

Results and Discussion

Steady Shear Rheology in 1.0 M Aqueous NaCl. Figure 1 shows the steady shear viscosity $\eta(\dot{\gamma})$ of X2F2 in 1.0 M aqueous NaCl plotted against shear rate $\dot{\gamma}$ for several solutions, most of which have $W \leq W_i$ and are completely isotropic in the quiescent state. Only for the most concentrated solution ($W = 6.79$) is the concentration slightly greater than W_i. All of the curves show strong shear-thinning behavior at high shear rates. The least concentrated solutions approach a Newtonian plateau at the lowest accessible shear rates. In contrast, Newtonian behavior dominates in the concentration range $W \leq W_i$ for the low molecular weight sample X13F3. None of the curves in Figure 1 displays a shear thinning region at low shear rates that is observed for some samples of X13F3 in Figure 4 of the preceding paper.

The viscosity at low shear rates increases steadily with increasing concentration in Figure 1, as is normally observed for isotropic polymer solutions. At high shear rates, the increase in viscosity is much less pronounced and almost vanishes. Indeed, the solution of highest concentration ($W = 6.79$) shows a reversal of this trend in the shear thinning region at intermediate $\dot{\gamma}$. Figure 2 displays the dependence of $\eta(\dot{\gamma})$ on $\dot{\gamma}$ for X2F2 solutions in the biphasic regime in the quiescent state; the curve for $W = 6.79$ from Figure 1 is repeated. In this concentration range, the viscosity at low shear rates *decreases* monotonically as the polymer concentration increases, because these samples contain an increasing volume fraction Φ of the less viscous anisotropic phase as the overall concentration W increases. The concentration dependence of the viscosity essentially vanishes at higher shear rates where the flow curves for the several concentrations effectively converge.

Figure 3 shows samples with $W \geq 8.70$ that are fully anisotropic in the quiescent state. As the concentration of the anisotropic solutions is increased, the flow curves become more complicated. Here there are three re-

* To whom correspondence should be addressed. Telephone +1 (949) 824-6019; Fax +1 (949) 824-8571; email dbrant@uci.edu.

10.1021/ma011527e CCC: $22.00
Published on Web 02/09/2002

Table 1. Exponent n Values of $\eta(\dot\gamma) = A\dot\gamma^{-n}$, $\eta^*(\omega) = A\omega^{-n}$, $G'(\omega) = A\omega^n$ and $G''(\omega) = A\omega^n$ for X2F2 in 1.0 M Aqueous NaCl[a]

W	$\eta(\dot\gamma)$			$\eta^*(\omega)$		$G'(\omega)$		$G''(\omega)$	
	Low $\dot\gamma$	Intermed $\dot\gamma$	High $\dot\gamma$	Low ω	High ω	Low ω	High ω	Low ω	High ω
2.87	0.173		0.590	0.04	0.400	1.335	0.695	0.898	0.541
3.64	0.131		0.627	0.168	0.491	1.109	0.554	0.702	0.455
4.30	0.191		0.667	0.291	0.520	0.913	0.496	0.571	0.433
5.04	0.249		0.679	0.353	0.532	0.835	0.479	0.510	0.429
5.60	0.702			0.466	0.580	0.607	0.417	0.398	0.408
6.24	0.712			0.524	0.592	0.561	0.399	0.366	0.413
6.49	0.715			0.545	0.611	0.515	0.379	0.341	0.407
6.79	0.718			0.550	0.613	0.476	0.378	0.328	0.406
6.99	0.629			0.465	0.567	0.523	0.430	0.399	0.428
7.27			0.572	0.337	0.508	0.674	0.516	0.555	0.468
7.47	0.436		0.540	0.301	0.473	0.779	0.558	0.635	0.484
8.32		0.088	0.520	0.097	0.383	1.137	0.723	0.861	0.580
8.70	0.107	- 0.048	0.512	0.079	0.368	1.129	0.765	0.874	0.599
9.53	0.263	- 0.111	0.500	0.078	0.340	1.178	0.828	0.904	0.607
10.99	0.385	- 0.147	0.435	0.073	0.319	1.167	0.877	0.920	0.629
12.00	0.421	- 0.165	0.413	0.067	0.290	1.158	0.935	0.908	0.660
12.73	0.498	- 0.181	0.409	0.071	0.290	1.182	0.947	0.906	0.659
14.17	0.455	- 0.195	0.384	0.073	0.240	1.116	1.025	0.936	0.722

[a] Bold horizontal lines separate solutions that, when quiescent, are isotropic (top), biphasic (middle), and anisotropic (bottom). Bold vertical line separates steady shear and oscillatory data.

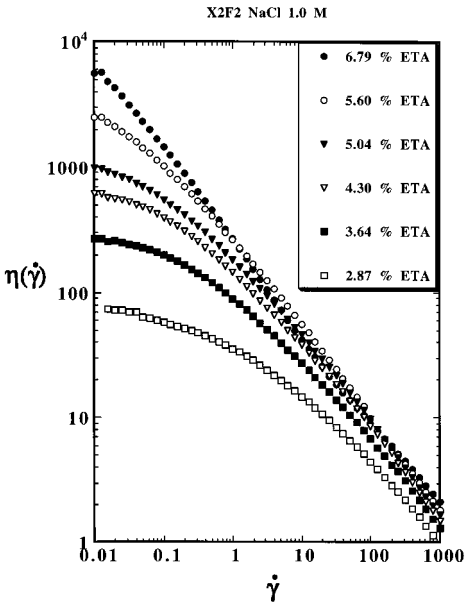

Figure 1. Steady shear viscosity $\eta(\dot\gamma)$ for X2F2 in aqueous NaCl at $C_s = 1.0$ M vs shear rate $\dot\gamma$ for several solutions, most of which have $W \le W_i$ and are fully isotropic in the quiescent state.

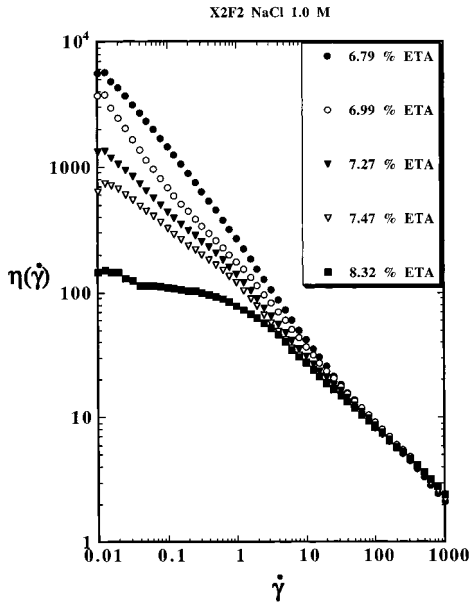

Figure 2. Steady shear viscosity $\eta(\dot\gamma)$ for X2F2 in aqueous NaCl at $C_s = 1.0$ M vs shear rate $\dot\gamma$ for solutions that are in the biphasic regime in the quiescent state.

gimes: shear-thinning behavior at low and high shear rate separated by a shear thickening domain in the approximate range $0.1 \le \dot\gamma \le 1.0$ s^{-1}. For X13F3 in 1.0 M aqueous NaCl, the shear-thickening regime for $W \ge W_a$ is also present, but it is much less pronounced.[1] The

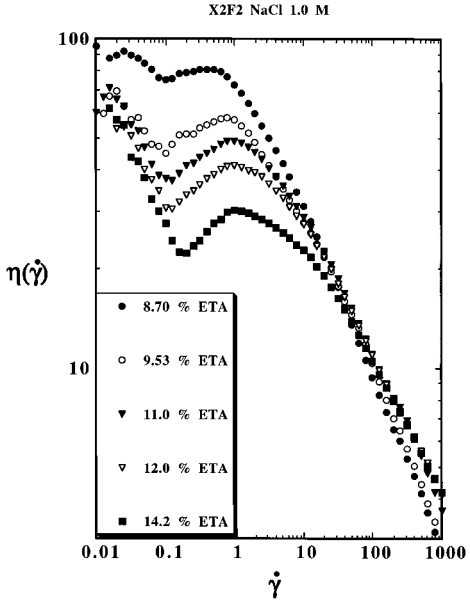

Figure 3. Steady shear viscosity $\eta(\dot{\gamma})$ for X2F2 in aqueous NaCl at $C_s = 1.0$ M vs shear rate $\dot{\gamma}$ for solutions that are in the fully anisotropic regime in the quiescent state.

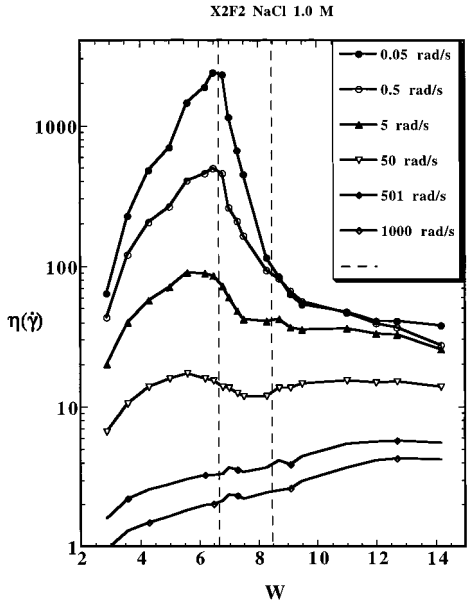

Figure 4. Steady shear viscosity $\eta(\dot{\gamma})$ for X2F2 in aqueous NaCl at $C_s = 1.0$ M vs concentration W for several shear rates. Vertical dashed lines indicate the phase boundary concentrations W_i and W_a in the quiescent state.

flow curves in Figure 3 converge and cross at $\dot{\gamma} \approx 40$ s^{-1}, i.e., the viscosity below 40 s^{-1} decreases with increasing concentration, whereas above 40 s^{-1} there is some increase with increasing concentration. Pseudoplasticity at low $\dot{\gamma}$ for the fully anisotropic solutions is reminiscent of region I behavior reported earlier for nematic lyotropic polymer liquid crystals, but it occurs here in solutions much less viscous than those normally associated with region I behavior ($\eta \geq 1000$ poise).[2] Shear thinning behavior at high $\dot{\gamma}$, often observed with lyotropic nematics (region III), appears prominently throughout the concentration range covered here. The nearly Newtonian behavior of the least concentrated anisotropic solutions at low $\dot{\gamma}$ appears consistent with earlier reports of the behavior of polymer lyotropic nematics in region II, but the shear thickening behavior seen here for the highly concentrated solutions at intermediate $\dot{\gamma}$ has seldom been reported.[3]

This shear thickening is clearly a reflection of the complex rheology of the textured structures in fully anisotropic solutions[3−7] and we believe it is likely to be associated with the negative first normal stress difference N_1 observed at intermediate shear rates in other lyotropic liquid crystalline phases.[8−11] Negative values of N_1 have been attributed to a shear-induced distortion of the orientation distribution function causing it to be less anisotropic than in the absence of shear.[2,4,5] In this regime of $\dot{\gamma}$, with progressively increasing $\dot{\gamma}$ the distribution function is increasingly disrupted relative to the quiescent state, so the power dissipated per unit volume in shearing the sample increases with $\dot{\gamma}$. At sufficiently large $\dot{\gamma}$, alignment due to shear dominates over spontaneous alignment, and the more conventional (region III) pseudoplastic behavior is restored.

The flow curves have been fitted by a power law $\eta(\dot{\gamma}) = A\dot{\gamma}^{-n}$ in three different shear rate ranges. The corresponding exponents are listed in columns 2−4 of Table 1 (compare with Table 3 of the preceding paper).[1] For some concentrations, it was not possible to obtain meaningful exponents in all shear rate ranges. For X2F2, as for X13F3, in the high shear rate range the power law exponents increase with W up to W_i, and then decrease with further increase of W. For solutions with $W \geq W_a$, the exponents increase with W in the low shear rate range but decrease in the high shear rate range.

The data of Figures 1−3 are conveniently summarized in Figure 4, where the viscosities at several fixed shear rates are plotted as a function of polymer concentration. Vertical dashed lines identify W_i and W_a for the quiescent solutions. The peak in these plots, which is close to W_i at low shear rate, moves to lower W as $\dot{\gamma}$ increases. The shear rate dependence of $\eta(\dot{\gamma})$ is clearly much more pronounced than for X13F3 (compare Figure 6 of the preceding paper).[1] There are very strong dependences of $\eta(\dot{\gamma})$ on W below W_a at low shear rates. Above W_a, however, $\eta(\dot{\gamma})$ becomes relatively independent of concentration. This is distinctly different from the behavior reported for still higher molecular weight xanthan samples for which the viscosity is reported to increase with increasing W beyond W_a.[12,13] For X2F2 a sharp increase in $\eta(\dot{\gamma})$ with W in the range below W_i is followed by an even more abrupt decline in $\eta(\dot{\gamma})$ with W across the concentration range of biphasic quiescent solutions. The peak in η near W_i is erased at high shear rates, however. Under high shear stress there is little, if any, distinction between the isotropic and anisotropic phases, and $\eta(\dot{\gamma})$ just increases monotonically with W until the chains achieve an asymptotic degree of alignment. In contrast to X13F3, the present sample is not Newtonian under steady shear for $W \geq W_a$.

Oscillatory Rheology in 1.0 M Aqueous NaCl. Oscillatory shear data plotted as $\eta^*(\omega)$ against ω across the concentration range $2.87 \leq W \leq 14.17$ are similar to the plots of $\eta(\dot{\gamma})$ against $\dot{\gamma}$ shown in Figures 1−3 within the same frequency/shear rate range (the highest accessible frequency was 100 s^{-1}). The frequency dependence of $\eta^*(\omega)$ can be analyzed in the same way as for $\eta(\dot{\gamma})$, and the power law exponent values n are given in Table 1. As can be seen from those n values, when the concentration is low there is a Newtonian plateau region for $W = 2.87$ at low frequency. That low frequency Newtonian plateau feature disappears very quickly with the increase of concentration. The low-

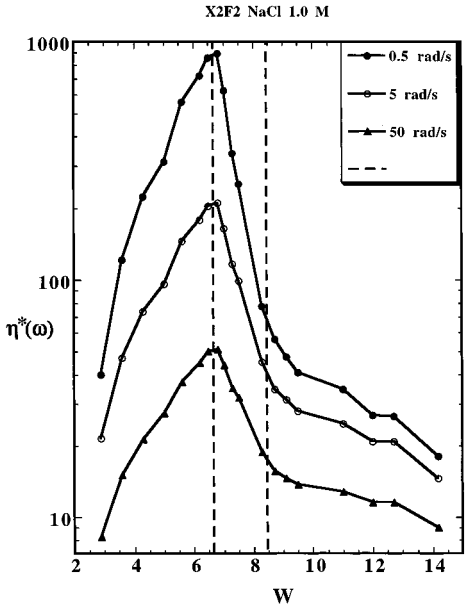

Figure 5. Plot of oscillatory shear viscosity $\eta^*(\omega)$ for X2F2 in aqueous NaCl at $C_s = 1.0$ M vs concentration W for several frequencies. Vertical dashed lines indicate the phase boundary concentrations W_i and W_a in the quiescent state.

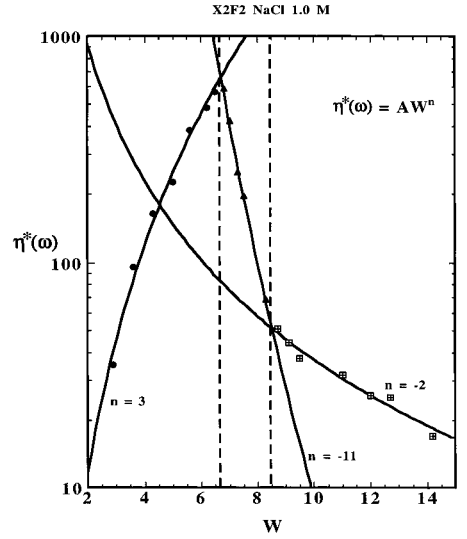

Figure 6. Demonstration of phase boundary concentration determination from power law plots of dynamic viscosity $\eta^*(\omega)$ for X2F2 in aqueous NaCl at $C_s = 1.0$ M vs W for frequency $\omega = 0.5$ Hz. Vertical dashed lines indicate the phase boundary concentrations W_i and W_a in the quiescent state. Power law exponents n are shown for each domain of the phase diagram.

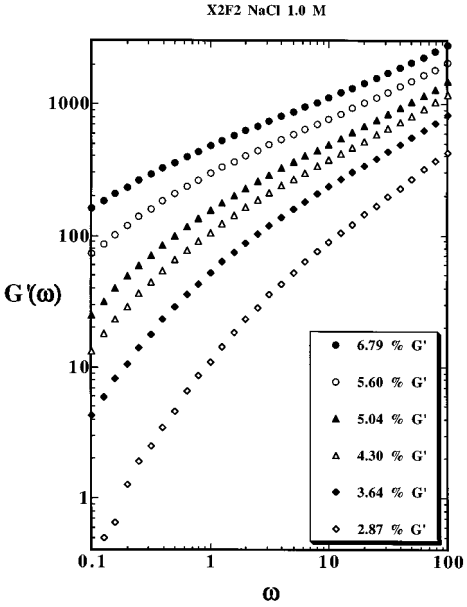

Figure 7. Storage modulus $G'(\omega)$ for X2F2 in aqueous NaCl at $C_s = 1.0$ M vs frequency ω for several solutions, most of which have $W \leq W_i$ and are fully isotropic in the quiescent state.

frequency exponent peaks at $W = 6.79$ and then decreases with further increase of W until reaching almost zero when $W \geq W_a$, in which region the flow curves show significant Newtonian plateau behavior at low frequency and are quite different from the corresponding flow curves obtained from steady shear experiments. They are simpler in appearance and, notably, do not have a shear thickening region at intermediate frequencies separating two shear thinning domains. Apparently disruption at intermediate ω of the orientation distribution function characteristic of the quiescent phase does not occur in oscillatory shear, at least not in the linear viscoelastic regime.

Plotting $\eta^*(\omega)$ against concentration W results in Figure 5, which can be compared directly with the corresponding plot for the steady shear results in Figure 4. In oscillatory shear, the viscosity maximum occurring near W_i does not change position as ω increases. Whereas this maximum is eliminated at high shear rate in Figure 4, it survives to the highest accessible frequencies in the oscillatory measurements. For $W \geq W_a$, $\eta^*(\omega)$ continues to decline as W increases, while $\eta(\dot{\gamma})$is generally increasing or constant with W in this concentration range. Using a power law representation of the data in the form $\eta^*(\omega) = AW^n$ in each concentration regime, one can use the results in Figure 5 to identify rather accurately the concentrations W_i and W_a that characterize the isotropic and anisotropic phases in quiescent biphasic systems. It can be seen in Figure 6 that the intersections of the power law curves occur very close to W_i and W_a; the data at $\omega = 0.5$ s^{-1} were used to prepare Figure 6. Similar observations were reported for sample X13F3.[1]

The loss tangent exceeds unity for nearly all of the X13F3 solutions studied in the previous paper,[1] but that is not the case for X2F2. Figures 7−9 show the curves of elastic modulus $G'(\omega)$ vs frequency ω for all the solutions studied. $G'(\omega)$ increases with W in the isotropic regime but decreases with W for the biphasic and, less dramatically, the anisotropic solutions. Fitting the curves with the power law $G'(\omega) = A\omega^n$ gives exponent n values which are compiled in Table 1, where the high and low-frequency regimes are reported separately. The exponent n decreases with increasing frequency at all concentrations, and the limiting high-frequency values are rather dependent on W in all concentration regimes. For the isotropic solutions the limiting exponents do not appear to match those expected for rigid or semiflexible polymers in dilute solution.[14,15] The exponents at both high and low frequency decrease with W for isotropic solutions but increase with W in the biphasic regime. For anisotropic solutions the low frequency exponent is essentially constant with W, while it increases with W at high frequency.

Figure 10 summarizes the dependence of $G'(\omega)$ on W at $C_s = 1.0$ M for several values of ω. Vertical dashed lines identify the concentrations W_i and W_a for quiescent

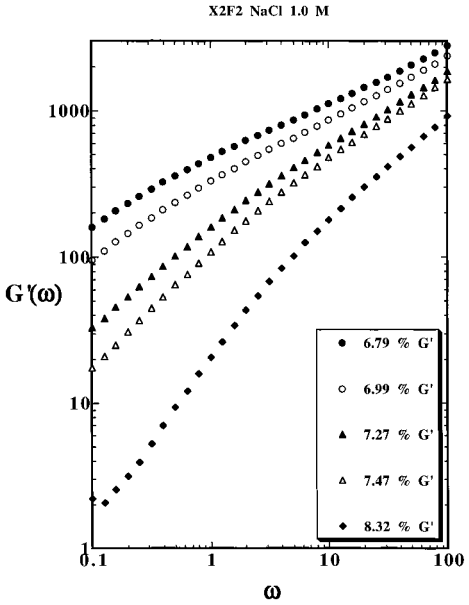

Figure 8. Storage modulus $G'(\omega)$ for X2F2 in aqueous NaCl at $C_s = 1.0$ M vs frequency ω for solutions that are in the biphasic regime in the quiescent state.

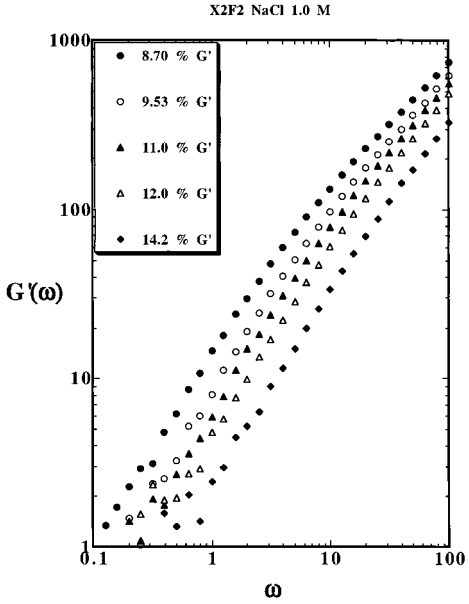

Figure 9. Storage modulus $G'(\omega)$ for X2F2 in aqueous NaCl at $C_s = 1.0$ M vs frequency ω for solutions that are in the fully anisotropic regime in the quiescent state.

solutions. Higher frequency curves consistently lie above those for lower frequencies in contrast to what is observed for steady shear/complex viscosity shown in Figures 4 and 5. All the curves of $G'(\omega)$ vs W have maxima close to the phase boundary concentration W_i determined by phase separation in the absence of shear. At any given frequency $G'(\omega)$ rises rapidly with increasing concentration of xanthan until the maximum is reached at $W = 6.79$, above which the elastic modulus drops quickly to a regime of reduced concentration dependence at concentrations above W_a. Fitting $G'(\omega)$ vs W with the power law $G'(\omega) = AW^m$ in each of the concentration ranges $W = W_i$, $W_i \leq W < W_a$, and $W \geq W_a$ yields curves that intersect very close to W_i and W_a just as in Figure 6.

The curves of loss modulus $G''(\omega)$ vs ω for X2F2 at $C_s = 1.0$ M are similar to Figures 7−9 and are not shown

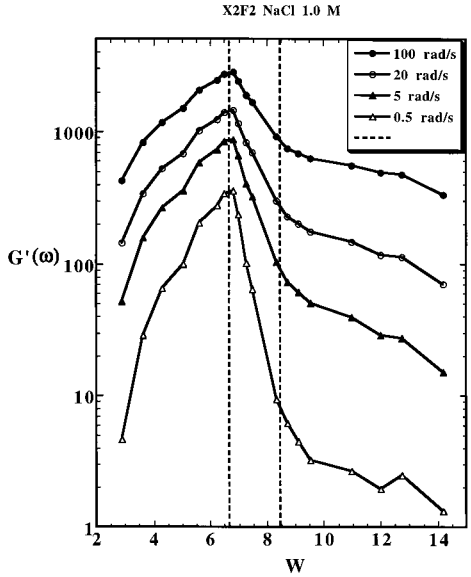

Figure 10. Storage modulus $G'(\omega)$ for X2F2 in aqueous NaCl at $C_s = 1.0$ M vs concentration W for several frequencies. Vertical dashed lines indicate the phase boundary concentrations W_i and W_a in the quiescent state.

here. $G''(\omega)$ increases monotonically with increasing frequency, and the curves can be fitted with the power law $G''(\omega) = A\omega^n$ at high and low frequency; the exponent values n are tabulated in Table 1. At low frequency, n decreases very fast with increasing concentration until it reaches a minimum at $W = 6.79$ whereupon it rises even more quickly with concentration to reach a roughly constant value above $W = 8.32$. For X2F2 the relationship between loss modulus $G''(\omega)$ and W at $C_s = 1.0$ M mimics the W dependence of $G'(\omega)$ shown in Figure 10 with a peak at $W = 6.79$. Separate power law fits to the data in the concentration ranges $W = W_i$, $W_i \leq W < W_a$, and $W \geq W_a$ produce curves that cross near W_i and W_a just as do the similar power law fits to $\eta^*(\omega)$ and $G'(\omega)$.

For a Newtonian polymeric fluid the power law exponent values for rheological parameters $\eta(\dot{\gamma})$, $\eta^*(\omega)$, $G'(\omega)$, and $G''(\omega)$ as functions of $\dot{\gamma}$ or ω are 0, 0, 2, and 1, respectively.[2,14] For gels, both $G'(\omega)$ and $G''(\omega)$ become independent of ω with $G' \gg G''$, and $\eta^*(\omega)$ declines with power law exponent -1.[14,16] Experimental deviations from these limiting exponent values can serve as an index of the polymer−polymer interactions; i.e., they provide information about structure in the polymer solution. Sample X13F3 at $C_s = 1.0$, 0.1, and 0.01 M shows essentially Newtonian fluid behavior as indicated by the exponent values given in Tables 3−5 of the previous paper, [1] which are close to the expectations for Newtonian fluids for all solutions studied. For sample X2F2 there are two sets of exponents, one characteristic of the low-frequency regime and the other characteristic of high-frequency behavior.

As shown for sample X2F2 at $C_s = 1.0$ M in Table 1, the fully anisotropic solutions are quite liquidlike at low frequencies as judged by the frequency dependences of $\eta^*(\omega)$, $G'(\omega)$, and $G''(\omega)$. In the isotropic regime, the low frequency exponent values for these oscillatory parameters change montonically away from the liquidlike limit toward the gellike limit with increasing concentration suggesting gradual network formation (transient gellike structure development) as concentration rises. In the biphasic region liquidlike behavior returns at low

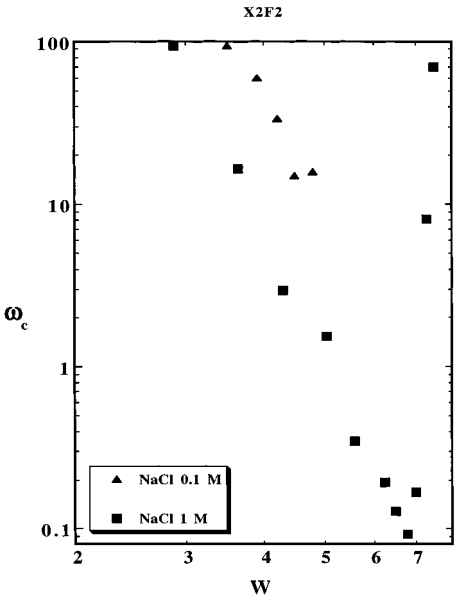

Figure 11. Crossover frequencies ω_c at which the loss tangent $\tan \delta = G''(\omega)/G'(\omega) = 1$ as a function of polymer concentration W for X2F2 in aqueous NaCl at $C_s = 1.0$ and 0.1 M.

frequency as concentration increases. Here transient network junctions present at low frequency in the more concentrated isotropic solutions are suppressed by the development of spontaneous alignment in the anisotropic phase, which grows in volume fraction Φ as W increases between W_i and W_a. The behavior at high frequency is generally more gellike than at low frequency, simply because the relaxation times of the transient interactions between the polymer chains are too long to permit disentanglements to occur on the time scale of the oscillations.

When plotted together against ω, the moduli $G'(\omega)$ and $G''(\omega)$ cross at a frequency ω_c that depends on the concentration W of X2F2 when $C_s = 1.0$ M. For $W = 2.87$, the smallest concentration studied, the loss modulus is always larger than the storage modulus except at frequency 100 s^{-1}. As the concentration is increased, $G'(\omega)$ becomes larger than $G''(\omega)$ at increasingly lower frequency. This trend in ω_c does not continue beyond W_i. On the other hand, the crossover frequency increases rapidly with increasing $W \geq W_i$ until it is out of the range of the instrument (>100 s^{-1} for the oscillatory experiment). Figure 11 shows a double logarithmic plot of ω_c vs W. The crossover frequency is seen to scale negatively with W in the range $W \leq W_i$. Cuvelier et al.[17] also observed this phenomenon for a higher molecular weight xanthan sample in 0.1 M aqueous NaCl. After passing the minimum at $W = 6.79$, the crossover frequency rises very rapidly with W and quickly passes out of the accessible frequency range for $W > 7.47$. The log curve looks like a distorted "V" with the minimum in ω_c corresponding to the phase boundary concentration W_i. The $G'(\omega)/G''(\omega)$ crossover can be observed only within a limited range of W and ω for a specific sample (in this case, X2F2 at $C_s = 1.0$ M). For the rigid rodlike xanthan sample X13F3, no $G'(\omega)/G''(\omega)$ crossover is observed in the accessible frequency range; see Figure 12 of the previous paper.[1]

Further Comparison of the Steady Shear and Oscillatory Results in 1.0 M Aqueous NaCl. Reference to the steady shear viscosity plot in Figure 4 shows that the peak at the lowest shear rate occurs very close to W_i, but with an increase in shear rate the peak shifts toward lower W. If the concentration at which $\eta(\dot\gamma)$ is maximal is interpreted as the isotropic−anisotropic phase boundary concentration W_i^γ at the corresponding shear rate in the steady shear mode, then the contribution of the shear field to the phase transition can be observed in the plots of Figure 4. For shear rates $\dot\gamma < 0.04$ s^{-1} $W_i^\gamma \approx W_i = 6.68$, but as the shear rate increases to 0.5 s^{-1}, W_i^γ falls to 6.49. When $\dot\gamma$ is increased to 50 s^{-1}, W_i^γ shifts further to 5.60. No peak is observed for shear rates $\dot\gamma = 316$ s^{-1} and above. In the shear regime $\dot\gamma \geq 500$ s^{-1}, alignment due to the shear field appears to dominate spontaneous excluded-volume-based alignment regardless of concentration. Apparently, X2F2 is aligned under the shear field much more readily than X13F3 described in the previous paper,[1] because for X13F3 the steady shear viscosity peak persists even at the highest shear rate $\dot\gamma = 1000$ s^{-1}.

Larson[5] argues on theoretical grounds that shear-induced transitions from the isotropic to the nematic state of a lyotropic system are not expected to occur unless the biphasic concentration regime is narrower than predicted by the Onsager theory.[18] For sample X2F2 at $C_s = 1.0$ M the measured ratio $c_a/c_i = 1.28$. The Onsager theory predicts this ratio to be 1.34 for very long, rodlike molecules. Elaborations of the Onsager theory[19] suggest other (smaller) values for c_a/c_i, for semiflexible, polyelectrolytes such as xanthan sample X2F2, but given the inherent approximations in the theory and the polydispersity of X2F2, one cannot expect to make quantitative comparisons here.

It is interesting to examine the relationship between $\eta(\dot\gamma)$ and $\eta^*(\omega)$ by superimposing shear rate and frequency ($\dot\gamma$, ω) as the abscissa and plotting $\eta(\dot\gamma)$ and $\eta^*(\omega)$ on the ordinate. Some representative plots appear in Figure 12. When the concentration is low ($W = 2.87$, 3.64, and 4.30 in Figure 12a), $\eta(\dot\gamma)$ is observed to cross below $\eta^*(\omega)$ as shear rate and frequency are increased. The crossover shear rate/frequency decreases with increasing concentration, reaching 0.2 s^{-1} for $W = 4.30$. Further increase in W pushes the crossover shear rate/frequency out of the accessible range so that in the more concentrated completely isotropic phases (e.g., $W = 6.49$ in Figure 12a) and in biphasic systems in which the isotropic phase predominates (e.g., $W = 6.79$ and 7.47 in Figure 12b) $\eta^*(\omega)$ is always greater than $\eta(\dot\gamma)$ at accessible frequencies. At still larger polymer concentrations in biphasic systems where the ansiotropic phase predominates (e.g., $W = 8.32$ in Figure 12b) or where a single anisotropic phase is present (e.g., $W = 9.53$ in Figure 12b), $\eta(\dot\gamma)$ exceeds $\eta^*(\omega)$ at low shear rate/frequency but again crosses below $\eta^*(\omega)$ at higher shear rate/frequency. For the fully anisotropic solutions, the crossover shear rate/frequency increases as W increases in contrast to the behavior of the isotropic systems. Consequently, for the more concentrated fully anisotropic phases studied $\eta(\dot\gamma) > \eta^*(\omega)$ at all accessible frequencies.

In sharp contrast to the lower molecular weight X13F3,[1] none of the X2F2 solutions obeys the Cox−Merz rule, which asserts that $\eta(\dot\gamma)$ and $\eta^*(\omega)$ should superimpose in plots against ($\dot\gamma$, ω) for polymeric solutions without "structure".[20] In the present systems solutions that are isotropic, and biphasic mixtures that are predominantly isotropic, display the condition $\eta^*(\omega) > \eta(\dot\gamma)$ over most of the accessible frequency range. In solutions that are anisotropic, and biphasic mixtures

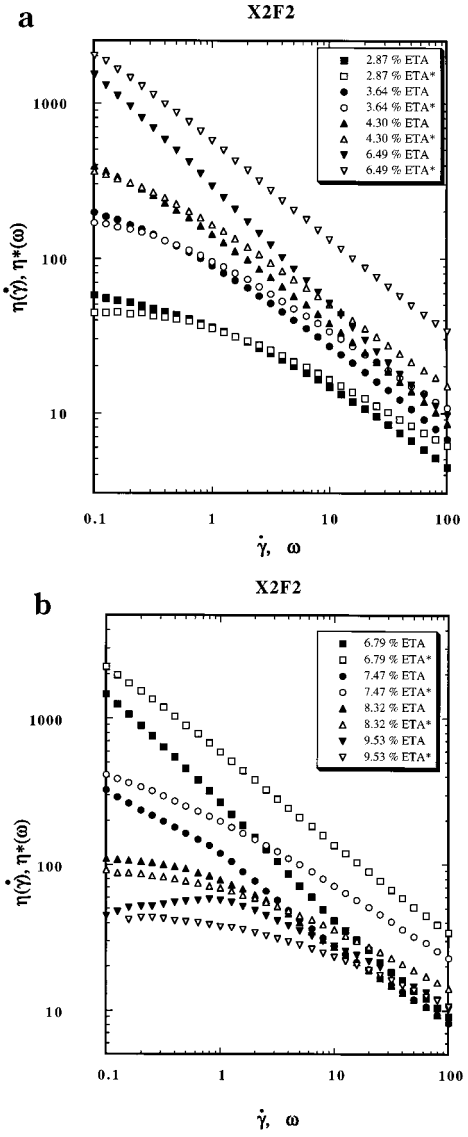

Figure 12. Steady shear ($\eta(\dot\gamma)$) and dynamic viscosities ($\eta^*(\omega)$) plotted against shear rate ($\dot\gamma$) and frequency (ω), respectively, for X2F2 in aqueous NaCl at $C_s = 1.0$ M for solutions in the isotropic regime (a) and for solutions in the biphasic and anisotropic regimes (b).

that are predominantly anisotropic, the inequality is reversed at most accessible frequencies. The behavior of the isotropic and predominantly isotropic systems clearly reflects the fact that shear thinning occurs at even at relatively low shear rate under steady shear but occurs to a lesser degree under oscillatory shear in the linear viscoelastic regime. In systems that are anisotropic, or predominantly so, it may be that more power is dissipated per unit volume in steady shear than in oscillatory shear because steady shear is more effective in disrupting the orientation distribution function of the liquid crystalline phase with the consequence that more power must be dissipated to align the molecules with the shear field.[2,4,5]

Steady Shear and Oscillatory Rheology in 0.1 M Aqueous NaCl. In 0.1 M aqueous NaCl ($C_s = 0.1$ M) the experiments covered the concentration range $1.16 \le W \le 10.06$ in order to embrace the biphasic region of the phase diagram and to explore the homogeneous domains on either side. (See Figures 2 and 3a and Table 2 of the previous paper.[1]) The flow curves for the steady shear experiments look similar to those shown in Figures 1−3 and are not presented here. At any low shear rate the value of $\eta(\dot\gamma)$ rises monotonically with W in the range $1.16 \le W \le 4.49$. At higher shear rate the viscosity for $W = 4.49$ (fully isotropic at rest) shows a reversal of this trend and falls below that of $W = 4.21$ at $\dot\gamma = 5$ s^{-1} and below that of $W = 3.90$ at shear rate 12 s^{-1}. This behavior, seen also for the most concentrated fully isotropic solutions of X2F2 and X13F3 when $C_s = 1.0$ M, again suggests that the shear field is contributing to the spontaneous alignment of the asymmetric molecules, i.e., that the phase boundary W_i^{γ} moves to lower values of W in the steady shear field.

The steady shear flow curve for $W = 1.16$ is quite different from the others and shows both a low and a high shear rate shear-thinning region with a Newtonian plateau in between. Shear thinning at low $\dot\gamma$, which is absent for $W \ge 2.16$, was also seen for sample X13F3 when $C_s = 1.0$ M for the least concentrated samples studied (see Figure 4 of the preceding paper).[1] It appears to be a characteristic of the least concentrated fully isotropic solutions studied here. As concentration is increased in the isotropic regime this feature disappears, but it may be present at shear rates below those accessible with the present equipment. All the curves for $W < W_i$ show a more extensive Newtonian plateau than does X2F2 at $C_s = 1.0$ M shown in Figure 1, but of course the concentrations are lower in the present case. Table 2 lists the exponent n values which are obtained by fitting the data with a power function of $\dot\gamma$. As in Figure 1 the upper frequency limit of the Newtonian region shifts steadily toward lower shear rates with increase in W.

For $W > W_i = 4.61$ at any shear rate below about 100 s^{-1}, $\eta(\dot\gamma)$ keeps decreasing with increasing W. The rate of decrease is larger in the biphasic regime than in the fully anisotropic regime. For $\dot\gamma > 100$ s^{-1}, $\eta(\dot\gamma)$ increases with W, although the increment is very small. The same phenomenon is observed for $W > W_i$ with X2F2 at $C_s = 1.0$ M in Figures 2 and 3. There the crossover frequency at which the concentration dependence of $\eta(\dot\gamma)$ changes sign occurs in the range $50 \le \dot\gamma \le 100$ s^{-1} for solutions that are biphasic or fully anisotropic when quiescent. When $C_s = 0.1$ M some plots of $\eta(\dot\gamma)$ against $\dot\gamma$ for concentrations in the biphasic regime display a complex shape that is not easily characterized. The same is observed for X2F2 at $C_s = 1.0$ M; see for example the curve for $W = 6.99$ in Figure 2. When $C_s = 0.1$ M, the Newtonian plateau feature at low $\dot\gamma$ persists for W closer to W_i than at $C_s = 1.0$ M as can be seen by comparing the exponent n values given in Tables 1 and 2. The power law exponent for $\eta(\dot\gamma)$ at high shear rate follows the same pattern in Tables 1 and 2: n increases with an increase in concentration to reach a maximum at W_i and then decreases rapidly with increasing concentration. The flow curves of solutions that are fully anisotropic when quiescent at $C_s = 0.1$ M do not show the shear-thickening regime seen in Figure 3 for the corresponding fully anisotropic solutions at $C_s = 1.0$ M.

A summary of the dependence of $\eta(\dot\gamma)$ on W for $\dot\gamma = 1$ and 50 s^{-1} is shown in Figure 13 for X2F2 at $C_s = 1.0$, 0.1, and 0.01 M. For $C_s = 0.1$ M, the peak shifts from $W = 4.79$ at low shear rate to lower W with an increase in $\dot\gamma$, and the peak disappears at still higher shear rate. This behavior suggests again that the phase boundary W_i^{γ} moves to smaller values of W with increasing shear

Table 2. Exponent *n* Values of $\eta(\dot\gamma) = A\dot\gamma^{-n}$, $\eta^*(\omega) = A\omega^{-n}$, $G'(\omega) = A\omega^n$, and $G''(\omega) = A\omega^n$ for X2F2 in 0.1 M Aqueous NaCl[a]

W	$\eta(\dot\gamma)$			$\eta^*(\omega)$		$G'(\omega)$		$G''(\omega)$	
	Low $\dot\gamma$	Intermed $\dot\gamma$	High $\dot\gamma$	Low ω	High ω	Low ω	High ω	Low ω	High ω
1.16	0.330	0.133	0.410						
2.16	0.067		0.601	0.092	0.259	1.33	0.984	0.892	0.644
3.00	0.044		0.687	0.108	0.378	1.40	0.757	0.878	0.559
3.50	0.049		0.747	0.103	0.432	1.43	0.661	0.881	0.522
3.90	0.076		0.752	0.139	0.450	1.36	0.605	0.796	0.503
4.21	0.062		0.763	0.189	0.478	1.18	0.569	0.738	0.479
4.49	0.080		0.765	0.232	0.496	1.09	0.537	0.697	0.467
4.79	0.213		0.674		0.493		0.531		0.476
5.21	0.475	0.066	0.600	0.188	0.367	0.954	0.763	0.794	0.577
5.64	0.079		0.477	0.028	0.286	1.672	1.068	0.933	0.653
6.06	0.009		0.361	0.045	0.238		1.194	0.922	0.699
7.33	0.066		0.324	0.049	0.155		1.362	0.921	0.710
8.01	0.047		0.325		0.100		1.392	0.907	0.722
8.83	0.058		0.342		0.155		1.355	0.921	0.743
10.06	0.046		0.308		0.089		1.577	0.937	0.777

[a] Bold horizontal lines separate solutions that, when quiescent, are isotropic (top), biphasic (middle), and anisotropic (bottom). Bold vertical line separates steady shear and oscillatory data.

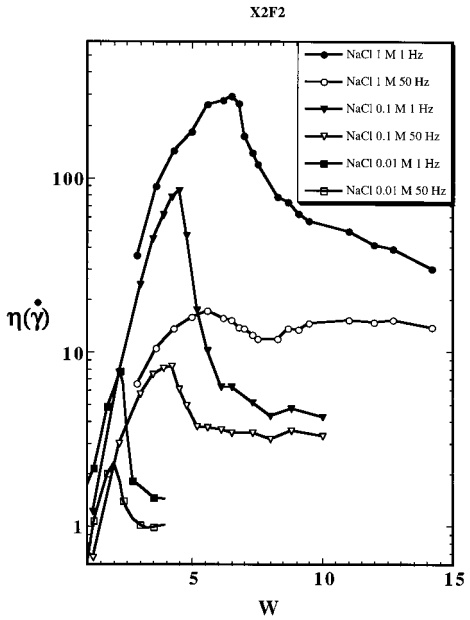

Figure 13. Steady shear viscosity $\eta(\dot\gamma)$ of X2F2 in aqueous NaCl at $C_s = 0.01$, 0.1, and 1.0 M vs concentration W for shear rates 1 and 50 Hz.

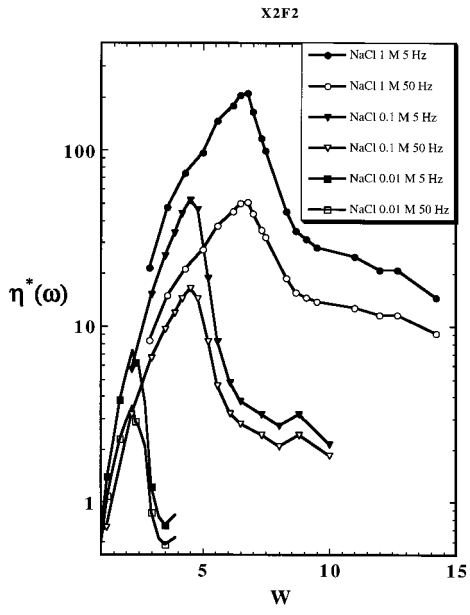

Figure 14. Dynamic viscosity $\eta^*(\omega)$ of X2F2 in aqueous NaCl at $C_s = 0.01$, 0.1, and 1.0 M vs concentration W for frequencies 5 and 50 Hz.

field for X2F2 at C_s = 0.1 M. Figure 14 similarly compares the dependence of $\eta^*(\omega)$ on ω for X2F2 at C_s = 1.0, 0.1, and 0.01 M. Here it is confirmed again by the data at all salt concentrations that, in contrast to the steady shear result, there is no shift in the peak of the plot of $\eta^*(\omega)$ against W as W increases. For $C_s = 0.1$ M, the maximum in $\eta^*(\omega)$ occurs at the same $W = 4.49$ for all frequencies, but the height of the peak decreases monotonically with increasing frequency. Variation of $\eta^*(\omega)$ with W can be fit by a power law $\eta^*(\omega) = AW^m$ in concentration ranges $W < W_i$, $W_i < W < W_a$, and $W > W_a$, and these curves cross very near W_i and W_a as already illustrated for other samples. Power law exponent n values for the $\eta^*(\omega)$ vs ω data are also in Table 2. The Newtonian plateau feature dominates both in

steady and oscillatory shear at low frequency. This is more apparent in Table 2 for the $\eta(\dot{\gamma})$ vs $\dot{\gamma}$ data than for the $\eta^*(\omega)$ vs ω data, simply because the lowest frequency available is 10 times greater than the lowest shear rate. For both types of data, the high-frequency exponent n values increase with W to a maximum around W_i and then decline steadily. Above W_a, the exponents are essentially constant as W increases. As expected, the oscillatory data show less shear thinning than the steady shear results.

When $\eta(\dot{\gamma})$ and $\eta^*(\omega)$ are plotted together against the corresponding shear rate/frequency ($\dot{\gamma}$, ω), they are found to behave very much like what is observed for X2F2 when $C_s = 1.0$ M (Figure 12), and the system departs from the Cox−Merz rule in this case also. The plots of $G'(\omega)$ and $G''(\omega)$ for X2F2 at $C_s = 0.1$ M against ω are similar to Figures 7−9 and are omitted. From the exponent n values in Table 2, we can see that X2F2 in 0.1 M aqueous NaCl has a more viscous liquid character than X2F2 in 1.0 M NaCl. The concentration dependences of $G''(\omega)$ and $G'(\omega)$ are just repetitions of those for X2F2 at $C_s = 1.0$ M and are discussed no further. The crossover frequencies for X2F2 at $C_s = 0.1$ M change in the same way with concentration as those for X2F2 at $C_s = 1.0$ M and are plotted together with the $C_s = 1.0$ M data in Figure 11. The lowest crossover frequency for X2F2 at $C_s = 0.1$ M is much higher than that for X2F2 at $C_s = 1.0$ M, and the concentration range showing $G''(\omega)$ and $G'(\omega)$ crossover is much narrower.

Steady Shear and Oscillatory Rheology in 0.01 M Aqueous NaCl. The rheology of isotropic, biphasic, and anisotropic X2F2 at $C_s = 0.01$ M was studied in the much lower concentration range, $1.00 \le W \le 3.95$. Because of the low polymer concentration, the torque produced at low shear rate/frequency was out of the range of the instrument used, and the accessible shear rate/frequency range was narrower than that for $C_s = 1.0$ and 0.1 M. For $C_s = 0.01$ M, the critical concentration at which $\eta^*(\omega)$ starts to decrease with increasing W is reduced to $W = 2.37$, but the general features of the flow curves for both steady shear and oscillatory shear look very similar to those for $C_s = 0.1$ M. The relationships between $\eta(\dot{\gamma})$ and $\eta^*(\omega)$ and W are shown, respectively, in Figures 13 and 14 for two different shear rates/frequencies. It can be seen that the curves at all three salt concentrations look similar to each other with a shifting of the peak position to lower W and reduction of peak height as the salt concentration decreases. For the solutions that are fully isotropic when quiescent, the curves do not overlap before reaching their respective maxima in contrast to the case for X13F3.[1] The data for $C_s = 1.0$ and 0.1 M can be compared in the range $3 \le W \le 4$, where it is seen that $\eta(\dot{\gamma})$ and $\eta^*(\omega)$ are larger at the higher salt concentration. In the range $1 \le W \le 3$, however, the viscosity is larger at the lower salt concentration. Occurrence of a "crossover concentration" above and below which the sensitivity of the viscosity of isotropic xanthan solutions to salt is reversed has been reported by others.[21] Those reports referred to xanthan solutions with $W = 1$ for samples that were presumably considerably higher in molecular weight than X2F2. Thus, the viscosity of X2F2 in the isotropic region depends on salt concentration, in a relatively complicated way. In the anisotropic domain viscosity increases with increasing salt concentration as described for X13F3.[1] The dependences of G' and G'' on W at $C_s = 0.01$ M are similar to those at higher salt concentration presented above and are not elaborated here.

For X2F2 solutions with $C_s = 0.01$ and $W \approx W_i$, the moduli $G'(\omega)$ and $G''(\omega)$ are observed to cross over at frequencies around the upper accessible limit of 100 s^{-1}. In general, the crossover frequencies are higher than those for X2F2 at $C_s = 1.0$ and 0.1 shown in Figure 11. As pointed out in the Introduction, the chains of sample X2F2 are semiflexible and wormlike. In an isotropic phase, the xanthan molecules are randomly oriented and an increase of xanthan concentration facilitates formation of a transient network by association or entanglement. Electrostatic screening plays an important role in determining the strength of this network. For X2F2 at $C_s = 0.01$, the screening effect is quite weak, so the anionic xanthan molecules are repelled from one another at relatively long range by their net negative charge. As a result, interchain contacts are weak and dissipate quickly. Hence they will be detected only at high frequency and any crossover to predominantly elastic behavior may occur at or above the upper measurable frequency of 100 s^{-1}. Addition of more electrolyte enhances the strength and longevity of the interactions. Thus at $C_s = 0.1$ and, especially at $C_s = 1.0$ M, the slower relaxation times for disruption of intermolecular contacts allow elastic response to dominate at relatively low frequencies. For all values of C_s investigated these systems pass back to predominantly viscous response as W exceeds W_i and some or all of the fluid consists of anisotropic domains with large order parameter and little tendancy for chain entanglements. Crossover to elastic dominance for the solutions with $W > W_a$ occurs at frequencies well outside the current experimental range even when $C_s = 1.0$ M (Figure 11).

Conclusion

When the xanthan concentration is increased past the critical concentration W_i, excluded volume effects require that xanthan molecules align to form an orientationally ordered phase. Molecules in the anisotropic phase are significantly aligned so that entanglements are greatly reduced, and incipient or transient network formation is suppressed. The rapidly decreasing branch of the crossover frequency curve in Figure 11 lies in the isotropic regime, the minimum corresponds very nearly to the concentration W_i, and the steeply increasing region lies in the biphasic regime. For sample X13F3 at $C_s = 0.01$, 0.1 and 1.0 M, there is no $G'(\omega)/G''(\omega)$ crossover observed at accessible frequencies, because the polymer chains are rigid and too short to form the kind of entanglement network detected for sample X2F2.

The zero-shear viscosity, η_0, of a series of xanthan samples at $C_s = 0.1$ M has been reported by Takada et al.[22] Takada reports that the exponent values in the power law function for $\eta_0 = AW^m$ are about 3 for his samples R-1 through R-3, 5.6 and 7.6 for samples R-4 and R-5, and 6−7 for samples R-6 through R-8. Using their data, we obtain exponents $m = 2.31$, 2.59, 3.11, 5.46, 7.14, 6.97, 8.05, and 8.17 for samples R-1 through R-8, respectively. These are plotted in Figure 15 together with our results for X13F3, X2F2, and X2F3 at $C_s = 0.1$ M with respective exponents $m = 2.56$, 4.63, and 3.12 (our own result for X2F3 not published elsewhere). It can be seen that the exponent changes slowly when the $M_w < 400\,000$ g/mol but increases steeply around $M_w = 500\,000$ g/mol and then ap-

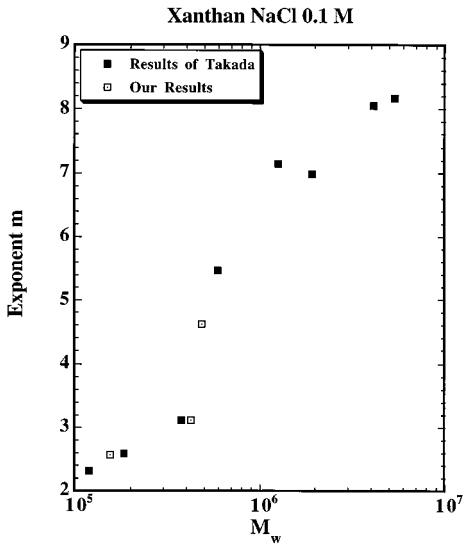

Figure 15. Scaling exponent m for the W dependence of steady shear viscosity $\eta(\dot{\gamma})$ vs weight average molecular weight M_w at low frequency for several xanthan samples in aqueous NaCl at $C_s = 0.1$M.

proaches a plateau around $M_w = 1\,000\,000$ g/mol. Thus, the concentration dependence of zero-shear viscosity depends on the molecular weight in a way that suggests a sharp increase in entanglement interactions for M_w between 400 000 and 1 000 000 g/mol for $C_s = 0.1$ M.

When $M_w < 300\,000$ g/mol, the polymer chains are short and quite rigid so that no substantial entanglement is possible. Hence, the exponent values $m \leq 3$, which is the range expected for rodlike molecules on theoretical grounds.[23] Solutions of low molecular weight xanthan should behave as viscous liquid as in the case for X13F3 ($M_w = 154\,000$, $N = L_w/2q = 0.33$). When the molecular weight is high (above 1 000 000 g/mol), the polymer chains are more flexible and can form an entanglement network that relaxes slowly even relative to a low-frequency perturbation, so the exponents m are above 7 and appear to approach some still larger asymptotic value. Sample X2F2 ($M_w = 480\,000$, $N = L_w/2q = 1.03$) has a mean contour length of approximately two persistence lengths. Even under low frequency perturbations its solutions display evidence of entanglements that do not dissipate rapidly relative to the shear rate ($m = 4.6$), and they show increasing evidence of short-lived entanglements as the shear rate is increased. High molecular weight xanthan is expected to have substantially more double helical imperfections than samples of lower molecular weight, and these imperfections represent the loci of particularly strong intermolecular interactions.[24] Solutions of ultrahigh molecular weight xanthan display, as expected, a more elastic than viscous character.[13] Between the two molecular weight extremes, there is a transition region corresponding to semiflexible wormlike polymer chains where there is some degree of entanglement, which is signified, for example, by the $G'(\omega)$ and $G''(\omega)$ crossover for sample X2F2. Hence, the proper choice of xanthan molecular weight is important in governing its behavior in various applications.

It is of interest to consider the interactions that dominate to produce spontaneous alignment of xanthan in the absence of shear. The strong dependence of phase boundary concentrations W_i and W_a on salt concentration (previous paper, Table 2)[1] suggests that electrostatic interactions are probably dominant in the range of C_s investigated here. This may not be true at still higher salt concentration, but the data available in Figure 2 of the previous paper[1] do not permit one to ascertain the salt concentration at which increases in W_i and W_a saturate with increasing C_s. It is useful in this regard to compare the values of W_i and W_a that are observed for the nonionic, triple helical polysaccharide schizophyllan (scleroglucan), which has nearly the same mass per unit length as xanthan. Itou et al.[25] have reported phase boundary concentrations in aqueous solution at room temperature for several schizophyllan samples including two (SPG and D40) with molecular weights close to those of X13F3 and X2F2. These concentrations, converted to weight percent W, are compared with those of X13F3 and X2F2 in Table 3. For the schizophyllan samples W_i and W_a are much larger, respectively, than they are for the corresponding xanthan samples, even at $C_s = 1.0$ M where the electrostatic interactions are screened to the greatest extent. The mass per unit length of schizophyllan is about 10% greater than that of xanthan, so rodlike xanthan double helices will have a contour length L_w about 10% greater than a schizophyllan triple helix of the same mass. Since the diameter of schizophyllan is perhaps 10% less than than that of xanthan,[26] xanthan and schizophyllan of the same molar mass will have nearly the same axial ratio. The small differences in axial ratio between SPG-3 and X13F3 and between D40 and X2F2 are not nearly large enough to explain why the boundaries of the biphasic region in schizophyllan occur at so much larger polymer concentrations.[27]

Direct measurements of forces between rodlike biological molecules have been reported by several workers.[26,28−30] Parsegian and co-workers have interpreted the repulsive forces at the range of surface separation ≤10−15 Å, measured using the osmotic stress technique

Table 3. Mean Surface-to-surface Separation of Rodlike Polysaccharides in the Anisotropic Phase at $W = W_a$[a]

Polymer/solvent system	W_i	W_a	Surface separation at $W = W_a$ in Å	Effective surface separation in Å
Schizophyllan SPG-3 in water M_w = 151,000, L_w = 71 nm	16.0	19.7	22	22
Xanthan X13F3 at C_s = 1.0 M M_w = 154,000, L_w = 79 nm	9.68	11.76	29	23
Xanthan X13F3 at C_s = 0.1 M M_w = 154,000, L_w = 79 nm	6.66	8.34	39	19
Xanthan X13F3 at C_s = 0.01 M M_w = 154,000, L_w = 79 nm	4.52	5.93	51	-9
Schizophyllan D40 in water M_w = 478;000, L_w = 223 nm	9.65	12.8	31	31
Xanthan X2F2 at C_s = 1.0 M M_w = 480,000, L_w = 247 nm	6.68	8.47	38	32
Xanthan X2F2 at C_s = 1.0 M_w = 480,000, L_w = 247 nm	4.61	6.30	48	28
Xanthan X2F2 at C_s = 1.0 M M_w = 480,000, L_w = 247 nm	2.15	3.11	79	19

[a] Bold horizontal line separates low (top) and intermediate (bottom) molecular weight samples.

in liquid crystalline samples of DNA, xanthan, and schizophyllan, as arising from the structuring of water at the surface of the polymer.[26] At these short distances of approach the force decays exponentially with separation with a decay length of approximately 3.3 Å, generally independent of polymer type, added electrolyte, or temperature. Although xanthan and schizophyllan display similar functional dependence on separation distance, repulsive forces between xanthan molecules were found to be 10 times greater than those between schizophyllan molecules in the same range of interaxial separation. This was interpreted to mean that the surface water on xanthan is organized more effectively around this charged polymer than around the neutral schizophyllan, thus rendering the repulsive forces larger in xanthan.[26]

The mean separation of molecular surfaces for schizophyllans SPG-3 and D40 and xanthans X13F3 and X2F2 at $W = W_a$ were calculated assuming the respective molecular diameters to be 22 and 20 nm, using a method described in the previous paper.[1] Results are reported in column 4 of Table 3. Because W_a is larger for schizophyllan than for xanthan at $C_s = 1.0$ M, the mean separation of schizophyllan molecules at W_a is smaller than for xanthan even at $C_s \leq 1.0$ M. If, however, the effective diameter of a xanthan molecule is taken to include the Debye radius of the surface charges, then the effective surface separation is similar (i.e., ≈20 Å for SPG-3 and X13F3 and ≈30 Å for D40 and X2F2) for the two polymers when xanthan is at $C_s = 1.0$ and 0.1 M; see column 5 of Table 3. This "correction" of the xanthan diameter suggests, however, that xanthan molecules at $C_s = 0.01$ M are effectively closer together at W_a than are the schizophyllan molecules in water. Given the significantly softer electrostatic potential associated with the xanthan surface charge at $C_s = 0.01$ M, it is perhaps not surprising that the xanthan molecules must achieve greater effective density before excluded volume forces are sufficient to provoke spontanous transition to the anisotropic phase. The general conclusion of this exercise is that the packing density of anisotropic xanthan and schizophylan rods at $W = W_a$ is very similar when xanthan is at $C_s = 1.0$ and 0.1 M. Under these conditions both the "hard" surface separation and the effective surface separation are larger by a factor of a least 2 compared to the range where hydration forces are postulated to be operative for stiff molecules.[26,30]

Osmotic stress studies have been extended to larger interaxial distances with DNA, and the data interpreted using an equation of state for polymer liquid crystals that incorporates contributions from hydration forces, electrostatic effects, and bending fluctuations.[31] DNA force−distance curves are dominated at short surface separation (≤15 Å) by the hydration term and are independent of ionic strength. At longer distances the repulsive force is dominated by conformational fluctuations. If the ionic strength is not too large, the fluctuation term carries an important electrostatic contribution. The data suggest, however, that screening of the electrostatic contribution saturates near $C_s = 1.0$ M, and the fluctuations work to enhance the core hydration terms only if the contour lengths of the molecules exceed their persistence lengths.[31]

This description of intermolecular interactions in DNA does not appear consistent with the current observations for xanthan. Sample X13F3 has a mean contour length of 79 nm, which is two-thirds of one persistence length (using $q = 120$ Å). Hence, if the above model for DNA interactions is applicable, the only contribution to the interaction of two X13F3 molecules at $C_s = 1.0$ M would be the hydration force, which has largely decayed away at the intersurface distances that characterize the fully anisotropic phase and moreso at the distances characteristic of the smaller concentration W_i where the anisotropic phase first appears. It seems clear from the strong dependence of W_i and W_a on C_s that electrostatic contributions to the excluded volume effect remain very important at $C_s = 1.0$ M. Likewise, both $\eta(\dot{\gamma})$ and $\eta^*(\omega)$ are strongly dependent on salt concentration for fully anisotropic X13F3 at any concentration observed (see Figures 12 and 13 of the previous paper).[1] Sample X2F2, in contrast, has a mean contour length that is approximately twice the persistence length. Fluctuation-enhanced repulsive hydration interactions might play a role here, but it should be recognized that because W_i and W_a are generally smaller for X2F2 than for X13F3, the mean axial distances in X2F2 solutions are even greater than those for X13F3. Here again W_i and W_a as well as $\eta(\dot{\gamma})$ and $\eta^*(\omega)$ for the anisotropic solutions depend strongly on C_s.

Acknowledgment. This work was supported by NIH Grant GM 33062. We thank Dr. Theresa M. McIntire for measuring the MWD of samples X2F2 and X13F3 using noncontact AFM.

References and Notes

(1) Lee, H.-C.; Brant, D. A. *Macromolecules* **2002**, *35*, 2212.
(2) Larson, R. G. *The Structure and Rheology of Complex Fluids*; Oxford University Press: New York, 1999.
(3) Yan, N. X.; Labes, M. M.; Baek, S. G.; Magda, J. J. *Macromolecules* **1994**, *27*, 2784−2788.
(4) Marrucci, G.; Maffettone, P. L. *Macromolecules* **1989**, *22*, 4076−4082.
(5) Larson, R. G. *Macromolecules* **1990**, *23*, 3983−3992.
(6) Walker, L. M.; Wagner, N. J.; Larson, R. G.; Mirau, P. A.; Moldenaers, P. *J. Rheol.* **1995**, *39*, 925−952.
(7) Walker, L. M.; Mortier, M.; Moldenaers, P. *J. Rheol.* **1996**, *40*, 967−981.
(8) Kiss, G.; Porter, R. S. *J. Polym. Sci., Polym. Symp.* **1978**, *65*, 193−211.
(9) Kiss, G.; Porter, R. S. *J. Polym. Sci., Polym. Phys. Ed.* **1980**, *18*, 361−388.
(10) Navard, P. *J. Polym. Sci., Polym. Phys. Ed.* **1986**, *24*, 435−442.
(11) Moldenaers, P.; Mewis, J. *J. Rheol.* **1986**, *30*, 567−584.
(12) Allain, C.; Lecourtier, J.; Chauveteau, G. *Rheol. Acta* **1988**, *27*, 255−262.
(13) Oertel, R.; Kulicke, W.-M. *Rheol. Acta* **1991**, *30*, 140−150.
(14) Ferry, J. D. *Viscoelastic Properties of Polymers*, 3rd ed.; John Wiley and Sons: New York, 1980.
(15) Carriere, C. J.; Amis, E. J.; Schrag, J. L.; Ferry, J. D. *J. Rheol.* **1993**, *37*, 469−478.
(16) Rodriguez, A. I.; Tecante, A. *Food Hydrocolloids* **1999**, *13*, 59−64.
(17) Cuvelier, G.; Launay, B. *Carbohydr. Polym.* **1986**, *6*, 321−333.
(18) Onsager, L. *Ann. N.Y. Acad. Sci.* **1949**, *51*, 627−659.
(19) Odijk, T. *Macromolecules* **1986**, *19*, 2313−2329.
(20) Dealy, J. M.; Wissbrun, K. F. *Melt Rheology and Its Role in Plastics Processing*; Van Nostrand Reinhold: New York, 1990.
(21) Cheetham, N. W. H.; Norma, N. M. N. *Carbohydr. Polym.* **1989**, *10*, 55−60.
(22) Takada, Y.; Sato, T.; Teramoto, A. *Macromolecules* **1991**, *24*, 6215−6219.
(23) Doi, M. *J. Polym. Sci., Polym. Phys. Ed.* **1981**, *19*, 229−243.
(24) Oviatt, H. W. J.; Brant, D. A. *Macromolecules* **1994**, *27*, 2402−2408.
(25) Itou, T.; Van, K.; Teramoto, A. *J. Appl. Polym. Sci., Appl. Polym. Symp.* **1985**, *41*, 35−48.

(26) Rau, D. C.; Parsegian, V. A. *Science* **1990**, *249*, 1278−1281.
(27) Flory, P. J. *Adv. Polym. Sci.* **1984**, *59*, 1−36.
(28) Israelachvili, J.; Wennerström, H. *Nature* **1996**, *379*, 219−225.
(29) Strey, H. H.; Podgornik, R.; Rau, D. C.; Parsegian, V. A. *Curr. Opin. Struct. Biol.* **1998**, *8*, 309−313.
(30) Parsegian, V. A.; Rand, R. P.; Rau, D. C. *Proc. Natl. Acad. Sci. U.S.A.* **2000**, *92*, 3987−3992.
(31) Strey, H. H.; Parsegian, V. A.; Podgornik, R. *Phys. Rev. E* **1999**, *59*, 999−1008.

MA011527E